Predicting Grain Size of Fe Si Alloys Steel Sheet through Magnetic Properties and Machine Learning with XAI

JunSeo Ha¹, Ho Sung Jang², Sunmi Shin², Chang-Soo Park³*, and SeMin Park¹*

¹Material System Engineering, Pukyong National University, Busan 48513, Republic of Korea ²Smart Forming Process Group, KITECH, Ulsan 44776, Republic of Korea ³Functional Materials and Components Group, KITECH, Gangwon-do 25440, Republic of Korea

(Received 9 April 2025, Received in final form 5 September 2025, Accepted 8 September 2025)

Measuring the grain size of electrical steel is important for understanding its properties, but until now studies have attempted this using experimental equations or machine learning (ML), resulting in limited models. This study applied three ML and Explainable-AI (XAI) to analyze magnetic properties and identify key the factors most relevant to grain size prediction. Among the three tree-based models, $B4_Br/Bm$, $B10_Pcm$ were identified as key variables. It was also found that variables under B1, B4, B10 conditions accounted for 60% of the model explanation ratio. Final model was constructed using these variables. These findings demonstrate the potential of ML with XAI to predict grain size with fewer magnetic measurement.

Keywords: electrical steel, magnetic properties, grain size, machine learning, XAI

1. Introduction

Evaluation of Grain size is important in the steel manufacturing process. This is because grain size affects not only mechanical properties such as strength and ductility, but also several properties such as corrosion and magnetic properties, weldability, electrical performance, etc. This is well illustrated by the several relative equation, for instance Hall-Petch equation and the Magnetic Core Loss equation, etc.

In electrical steel used as the core material for motors and transformers, controlling grain size is essential, as it significantly affects both mechanical and magnetic properties. In the electrical steel manufacturing process, grain size is regularly measured to evaluate the quality of steel sheets. Also, it has been noted that rolling technology is limited to producing a 0.2 mm thick electrical steel sheet with a thickness of 0.1 mm or less in a single process, because when Si is high, a problem occurs in which it is difficult to lower the pressure reduction rate. Many studies aim that thinner sheet results in better magnetic properties of the sheet metal, i.e. lower losses.

so two rolling processes have studied [1-3]. As mentioned earlier in this study, since grain size has a great influence on the magnetic properties of the steel plate, it is necessary to study and evaluate the specimen by securing the thickness of 0.1 mm through two rolling processes in our paper.

In continuous electrical steel production, real-time grain size control is important to ensure uniform material properties. Magnetic measurement, which only requires the application of a magnetic field, has been widely explored as a non-destructive alternative for grain size evaluation [4-10]. With research in this field still in its early stages since the late 1990s, research has been conducted to find linear relationships and regression equations between magnetic properties of materials and grain size [4]. Some research, attempts have been made to quantify the relationship between magnetic properties such as core loss, permeability, and flux density and grain size [5, 6].

However, the challenge lies in the microscopy method's limitation to only a few millimeter-sized specimens, which does not reflect the average grain size of larger areas. Also, grain size is commonly measured for long time using optical microscopy, which involves mounting, polishing, and etching the samples. Thus this makes the rapid measurement of large areas a significant challenge.

©The Korean Magnetics Society. All rights reserved.

*Corresponding author: Tel: +82-51-629-6378 e-mail: newtain@pknu.ac.kr (SeMin Park) e-mail: zionzia@kitech.re.kr (Chang-Soo Park) This difficulty is compounded by variability, such as grain size alterations resulting from unexpected equipment changes, which often lead to deviations from the desired material specifications and lead to defects. It is difficult to determine, which conditions are related to the grain size, the interaction of various variables because there are AC measurements of the magnetic field, and in the case of AC, the conditions for applying the magnetic field from low frequency to high frequency ranging from hundreds to hundreds of thousands of Hz. In addition, the resulting values from each hysteresis loop provide many factors. AC various in frequency (Hz), and the parameters obtained from the hysteresis loop (coercivity, iron loss, flux density, etc.) are all potential factors. This results in over 100 variables to consider, as measuring just 10 frequencies typically made more than 10 derived parameters per frequency.

So, a solution to this challenge has been necessary. Quantitative analysis techniques have been developed until now. For example, since the early 2000s, research on predicting grain size using machine learning techniques such as Feed Forward Neural Networks (FFNN) has been actively tried. Recent grain size prediction have studied to incorporate not only magnetic properties but also various non-destructive testing data, such as ultrasonic and coda waves [7-10].

In continuous electrical steel production magnetic measurement is considered to be the most advantageous approach for enabling real-time grain size control, although various methods have been explored. To overcome this limitation, Explainable Artificial Intelligence (XAI) techniques such as Permutation Feature Importance (PFI) and Shapley Additive Explanations (SHAP) were introduced to identify the key magnetic properties contributing to grain size. These techniques are effective to offer insight into the influence and importance of each variable, these have been used in drug discovery and manufacturing and have been shown to be effective [11-13]. Also, studies were tried to predict the grain size of low carbon steel with a Bayesian ANN model by evaluating the importance of input variables through Reversible Jump Markov Chain Monte Carlo (RJMCMC) [14], and to evaluate the importance of variables in a model using SHAP analysis to influence the growth behavior of austenite grains in a reheating process [15].

To address this challenge, we have studied to solve the problem by using PFI and SHAP analysis, which are XAI techniques based on machine learning and deep learning to address the black box problem and improve model interpretability. Provided that the important factors are identified, an indirect method for measuring grain size

may be established, offering significant potential for efficient grain size evaluation in the continuous production of metallic materials such as steel. Although the reasoning behind AI-driven variable selection may be difficult to interpret, this approach could significantly reduce the defect rate in manufactured materials and contribute to a non-destructive grain size measurement process.

2. Design Framework and Experimental Procedure

Fig. 1 shows the flowchart of the entire process of training and optimizing the model, identifying highly descriptive input variables through XAI, and as a final step, formulating the relationship expression with grain size. The training and test datasets were randomly divided in a 70:30 ratio using scikit-learn's train-test-split, and the random seed was fixed to ensure reproducibility. As a result, a DataFrame with 165 input variables and approximately 100 rows was used for training and testing. To impute missing values in the input variables, Simple-Imputer, IterativeImputer, and KNNImputer from scikitlearn were applied, and their performance was evaluated using Mean Squared Error (MSE) with the Random-ForestRegressor (RFR) model. The DataFrame imputed by IterativeImputer showed the lowest MSE (Table 1), and was consequently selected for preprocessing. To enhance its performance, a LightGBM-based version of

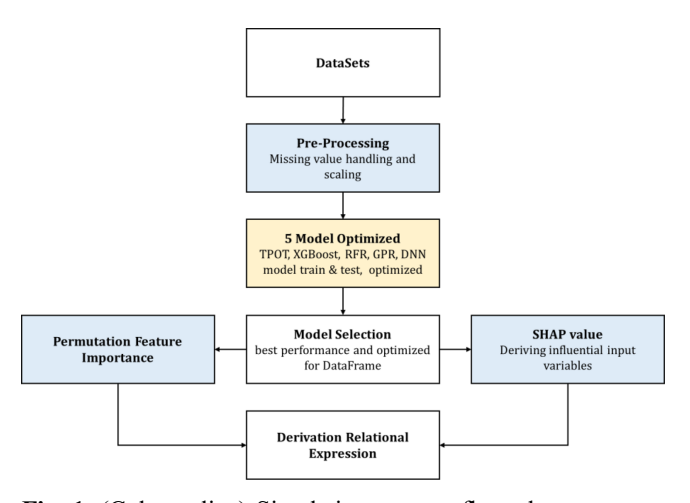


Fig. 1. (Color online) Simulation process flow chart.

Table 1. MSE comparison of Different Imputation Methods.

Model	MSE
IterativeImputer	284.17
kNNImputer	298.85
SimpleImputer	287.08

the IterativeImputer was employed, leveraging correlations among variables in an iterative manner. After imputation, MinMaxScaler was applied to normalize all feature values between 0 and 1, improving model training efficiency.

Five models were trained: eXtreme Gradient Boosting (XGBoost) [16], Deep Neural Networks (DNN) [17], Tree Based Pipeline Optimization Tool (TPOT) [18], Random Forest Regressor (RFR) [19], Gaussian Process Regressor (GPR) [20] The TPOT model, which is part of the AutoML package, is one of the models utilized in many machine learning studies, and the other four models are already used in many research fields that are related to materials science and engineering theory. These five models were subjected to hyperparameter optimization. XGBoost and RFR models were tuning using RandomizedSearchCV. DNN model was optimized using Adam and MSE loss function, with early stopping and cross-validation applied to prevent overfitting and evaluate performance via RMSE and R2. GPR model was optimized using Bayesian methods with Skopt's gp minimize, tuning the RBF kernel's length scale and noise level (alpha). TPOT, an AutoML tool, applied genetic programming to build and optimize pipelines consisting of feature engineering, hyperparameter tuning, and model evaluation. As the data were preprocessed beforehand, preprocessing operators were excluded by customizing the config dict. The R-Squared (R2) and Root Mean Square Error (RMSE) values of the five models were compared to selecting the best performing models and the three models optimized for DataFrame.

Following this, to increase the explanatory ability of the model, SHAP and PFI were used as XAI techniques. SHAP uses the Shapley value for each input variable to determine the SHAP value of the variable.

$$\varphi_i = \sum_{S \subseteq F} \frac{|S|!(|F| - |S| - 1)}{|F|!} (\nu_{S \cup \{i\}}(x_{S \cup \{i\}}) - \nu_S(x_S)) \quad (1)$$

 φ_i is the Shapley value of a particular input variable value, S is the set of input variables excluding a particular variable, F is the set of input variables including a particular variable, |S|, |F| are the sizes of the sets, and v_S is the predicted value of the machine learning model. These Shapley values help illustrate how a model predicts outcomes based on linear combinations of input features [15]. PFI is a method for evaluating how important a particular feature is to the performance of a prediction model [21]. This method measures the importance of each input variable by training a model and then randomly shuffling the values of certain features in the dataset and observing the effect on the model's performance.

$$PFI_{i} = rs - \frac{1}{J} \sum_{j=1}^{J} s_{i,j}$$
 (2)

The permutation importance PFI_i represents the impact of the *i*th variable, calculated as the difference between the model performance without shuffling (rs) and the average performance after shuffling the variable J times. This reflects the extent to which model performance degrades when that variable is altered. By applying XAI techniques, the black box nature of the models was addressed, and explanatory capability was improved by identifying key magnetic properties contributing most to grain size prediction and interpreting them through materials science. The library versions used for machine learning and optimization are scikit-learn 1.6.1 [22], SHAP 0.46.0 [11], and Python version 3.12.7. As a final step, the magnetic condition with the highest combined PFI and SHAP values was selected, a linear regression equation was derived using the corresponding input variables through ElasticNet, and modeling was performed using RFR.

In the experiments in this paper, a commercial specimen of 0.5 mm NO electrical steel was rolled to 0.1 mm. The SH-FU-80LTG instrument was used for heat treatment as shown in Table 2. Heat treatment was conducted under vacuum conditions ($\sim 10^{-4}$ torr). The specimens were inserted into a furnace that had been preheated to the target temperature, enabling rapid heating and allowing the specimens to reach the desired temperature within a short time. Since the specimens used in this study were very thin (0.1 mm), experimental measurements showed that they reached the target temperature within 2-3 minutes, corresponding to a heating rate of over 500°C/ min. The annealing time was defined as the duration after the specimen had reached the target temperature, and the heating period required to reach this temperature was excluded accordingly. After annealing, the specimens were air-cooled under vacuum conditions. The main elements are Si 0.6 wt% and Al 0.3 wt% by X-Ray Fluorescence Spectrometer (XRF). The instrument used for the analysis was an XRF from Rigaku (Rigaku/ZSX-Primus IV). The flux density, frequency, and notation are summarized in Table 3. The flux density is expressed in B

Table 2. Experimental conditions for heat treatment: time, temperature and vacuum level.

Annealing parameters	Time	Temperature	Vacuum level
values	0.2–44 min	800–1100 °C	$5 \times 10^{-4} \text{ torr}$



Fig. 2. (Color online) The size of the specimen used for magnetic measurements is 40×10 mm, and its thickness is 0.1 mm.

[Tesla] and the core loss is expressed in W [Watt/kg]. These fix parameters were chosen because they are frequently used in recent electrical steel performance studies. Several magnetic field conditions and low frequency 50 Hz to high frequency 20 kHz were set to reproduce the magnetic situation that is commonly encountered in actual motors and transformers. All measurements were tested using a single sheet tester (SST) to evaluate AC magnetic properties by various frequencies. The analysis was based on magnetic data obtained from hysteresis loops corresponding to different frequencies and magnetic field conditions. These measurement conditions are summarized in Table 4. At a given flux density and frequency condition, the following data are obtainable: $B_m(T)$, $B_r(T)$, $H_m(A/m)$, $H_c(A/m)$, $P_c(W)$, $P_{cv}(kW/m^3)$, $P_{cm}(W/g)$, μ_a , Br/Bm, $2\phi_m(Wb)$, phase(deg.). About 100 specimens were heat treated, and in the case of where the dependent variable grain size row was missing, the missing rows were processed using dropna. After preprocessing the missing data, a Data-Frame containing 165 input variables was then used for training and validation. The relationship between magnetic and electrical steel performance for the less commonly used magnetic properties: P_{cv} , P_{cm} , μ_a , $2\phi_m$, phase(deg.).

Table 3. Fixed parameters (Flux Density, Frequency) for measuring magnetic properties.

fix param	fix value	fix unit	freq (kHz)	Notation
Hm	100	A/m	0.05	B1
Hm	400	A/m	0.05	B4
Hm	800	A/m	0.05	B8
Hm	1000	A/m	0.05	B10
Hm	2500	A/m	0.05	B25
Bm	50	mT	20	W0.5/20000
Bm	100	mT	10	W1/10000
Bm	200	mT	5	W2/5000
Bm	500	mT	2	W5/2000
Bm	1000	mT	1	W10/1000
Bm	1000	mT	0.8	W10/800
Bm	1000	mT	0.4	W10/400
Bm	1000	mT	0.1	W10/100
Bm	1000	mT	0.05	W10/50
Bm	1000	mT	0.01	W10/10

is summarized in Table 4.

A total of 11 magnetic properties were measured using IWATSU's SY-8219 model, a single sheet tester and 0.1 mm thick electrical steel sheets were used. Since the specimen size for magnetic measurements is > 40 mm × 10 mm, the specimen was sized as shown in Fig. 2, the specimens were tested to size. Based on these data, a model was built to predict the grain size from the magnetic properties of the steel sheet.

Prior to the heat treatment and grain size measurement experiments, a phase field-based Finite Volume PDE Solver Using Python (FiPy) simulation [23] was conducted to identify grain growth tendencies under different heat

Table 4. Explain magnetic properties.

Properties	Related by electrical steel	Key determinants
$P_{cv}(kW/m^3)$	related to the efficiency of the transformer and motor core, lower	Steel sheet density, wt% Si, insulation coating,
(Core Loss per Volume)	losses increase efficiency and reduce heat generation	thickness
$P_{cm}(W/g)$	High power density motors and transformers require consider-	Density, silicon content, insulating properties
(Core Loss per Mass)	ation of lightweight core design	
μ_a	High permeability allows easy magnetic field transmission,	Grain size, crystal structure (Goss Texture), cold
(Absolute Permeability)	enhancing transformers and motor core performance.	working, and heat treatment.
Br/Bm	High values indicate greater hysteresis loss; reducing this is cru-	Texture, grain size, cold working.
(Remanence Ratio)	cial in low-loss steel sheets.	
$2\phi_m(Wb)$	Used to analyze the magnetic properties of the core in transform-	Magnetic field strength, core shape, frequency.
(Double Maximum Mag-	ers.	
netic Flux)		
phase(deg.)	High phase difference indicates significant energy loss, which is	Magnetic resistance, hysteresis properties, fre-
(Phase Difference)	more affected as frequency increases.	quency.

treatment conditions and to optimize the heat treatment parameters for improved experimental efficiency. The Phase Field model is a computational framework that models microstructural changes inside a material using a continuous phase variable (ϕ) to predict the growth behavior of complex microstructures over time. FiPy is a Python-based software that enables thermodynamically based simulations using the finite volume method [23].

$$F = \int_{V} [f_{bulk}(\phi) + f_{gradient}(\phi)] dV$$
 (3)

The free energy density function, F, represents the thermodynamic stability of ϕ driven by the simulation. $f_{bulk}(\phi)$ drives the system to converge to a phase with lower energy, Interface energy term, and the interface energy term, $f_{gradient}(\phi)$ represents the spatial variation of the interface at the phase boundary. These two terms are used to predict how the microstructure of a material changes under specific conditions using the above equation.

$$\frac{gu}{gt} = \varepsilon^2 \Delta u - f(u) \tag{4}$$

The Allen-Cahn equation is used to model phase transformations and the movement of phase boundaries by tracking changes in the state variable over time [24]. In this model, ε controls interfacial energy, and f(u), derived from potential energy, drives the system toward stability. The simulation is applied to predict grain growth and the resulting grain size distribution under various heat treatment conditions. The FiPy library used for the simulations was version 3.4.5.

To measure the grain size of the specimen, the

specimen was polished by electropolishing followed by etching with nital solution. The electrolyte for electropolishing, a mixture of glacial acetic acid (99.5%) and perchloric acid (60.0%) in a 3:1 ratio, was used. Electropolishing was employed using a BUEHLER ElectroMet4 device. The specimen was then etched in a 5% dilution of nitric acid in ethanol (nital solution) for 90 seconds. All processes were performed at room temperature (23 ± 2 °C). The microstructure was observed at $100 \times$ magnification using an optical microscope, and average grain size was determined from nine randomly selected areas per specimen using the linear intercept method in accordance with ASTM E112.

3. Results and Discussion

Fig. 3 shows the grain growth simulation results using FiPy at 800 °C, 950 °C, and 1100 °C according to heat treatment time. In Fig. 3(a), the heat treatment condition involves heating from room temperature (25 °C) to each target temperature over 10 seconds, followed by holding at that temperature for 240 seconds. Cooling is then carried out back to room temperature over a period of 60 seconds. The simulated average grain sizes at each temperature were 25.01 μ m, 46.62 μ m, and 83.25 μ m, respectively. As shown in Fig. 3(b), when compared with the experimental results, the largest difference was observed at 1100 °C, with a deviation of 6.1 μ m.

Fig. 4 shows the grain size measurements extracted from the total heat treatment conditions specifically at 1, 2, 3, 4, 6, 8, 12, 16, and 20 minutes for each temperature. At 1100 °C, heat treatment was performed only for 1, 2, and 3 minutes. The grain size showed a gradual increase as the temperature increased from 800 °C to 1100 °C.

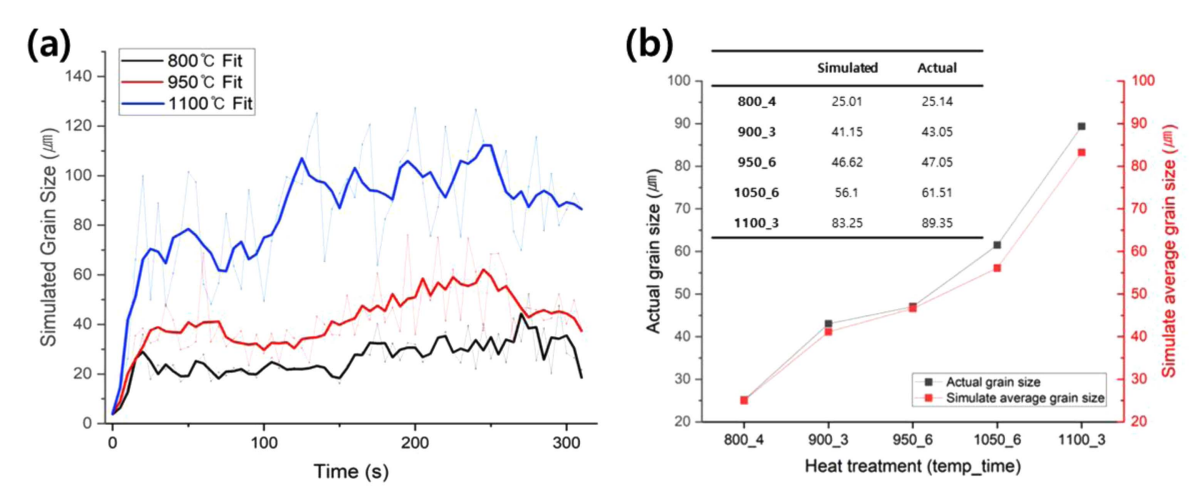


Fig. 3. (Color online) Results of the grain growth simulation using FiPy (a) at 800 °C, 950 °C, 1100 °C, (b) comparison between experimental values and simulation results.

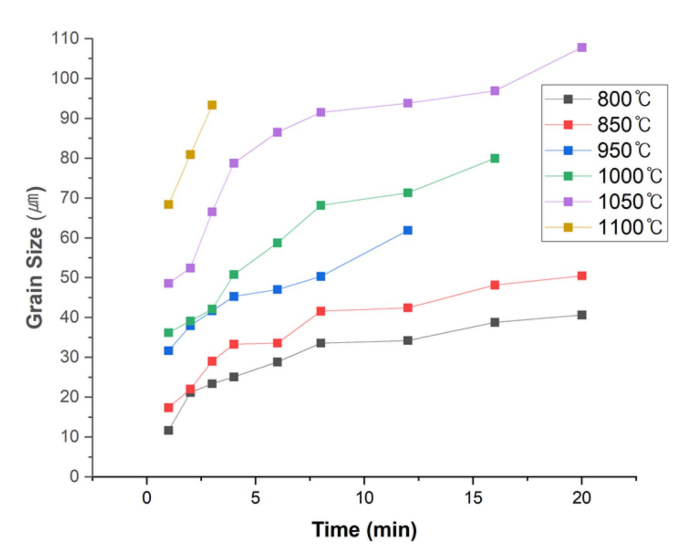


Fig. 4. (Color online) Optical micrographs of cold rolled specimens after annealing at (a) 800 °C, (b) 850 °C, (c) 900 °C, (d) 950 °C, (e) 1000 °C, (f) 1050 °C, (g) 1100 °C.

Grain size was observed using an optical microscope, as shown in Fig. 5. At temperatures above 1050 °C, grain

growth and recrystallized phenomena leading to irregular and large grain boundaries are observed. The heat treatment conditions at each temperature were set based on the FiPy simulation results, which allowed us to produce specimens with different grain sizes.

The final pipeline for the TPOT model is shown in Fig. 6 as a flowchart. This pipeline is a regression model with stacking. The first pipeline cross-validated the Ridge regression, and the second and third pipelines used the ExtraTreesRegressor regression model. This model is like RandomForest but differs in that it randomizes the selection of features and split points during tree generation. This has the advantage of helping to reduce the variance of the model, which prevents overfitting. The final pipeline uses the Elastic Net model, which uses L1 regularization to simultaneously control feature selection and regularization in regression. The hyperparameters in each model were optimized using AutoML. Subsequently, the hyperparameters in each model were optimized using different techniques: RandomizedSearchCV for the RFR and XGBoost models, Bayesian optimization for the GPR model, and the Adam optimizer with the MSE loss

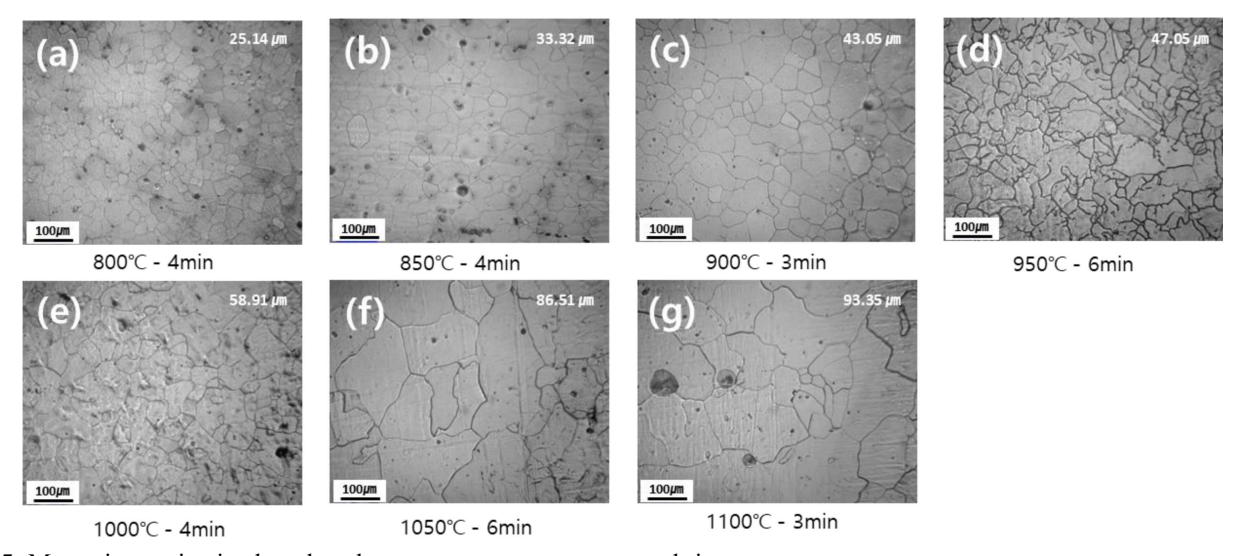


Fig. 5. Measuring grain size based on heat treatment temperature and time.

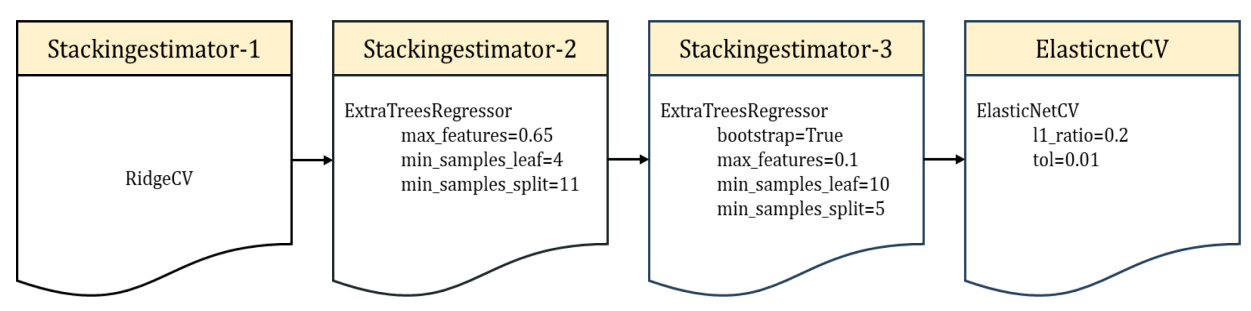


Fig. 6. (Color online) Optimized TPOT pipeline.

Table 5. Model performance comparison.

	TPOT	XGBoost	RFR	GPR	DNN
R2	0.75	0.79	0.74	0.71	0.73
RMSE	14.63	12.64	16.4	17.19	13.1

function for the DNN model.

Table 5 compares the R2 and RMSE values of the models. After modeling and optimization, the best performing model is XGBoost, which has the highest R2 (=0.79) and the lowest RMSE (=12.64). GPR recorded the lowest R2 (=0.71) and the highest RMSE (=17.19). This may be because GPR is vulnerable to noise or complex interactions among high-dimensional variables,

and the amount of data may not have been sufficient. When comparing the results of tree-based models (TPOT, XGBoost, RFR), the average R2 value was 0.76 and the average RMSE was 14.56. In contrast, the neural network-based models (GPR, DNN) showed relatively lower performance, with an average R2 of 0.72 and RMSE of 15.15.

The input variables selected for the PFI of each model were compared and analyzed to assess whether the model predictions could be explained based on material properties. A higher PFI value indicates a greater contribution of the variable to the model's performance. In addition, the SHAP values of each model were compared and analyzed to understand the explanatory capability of the models

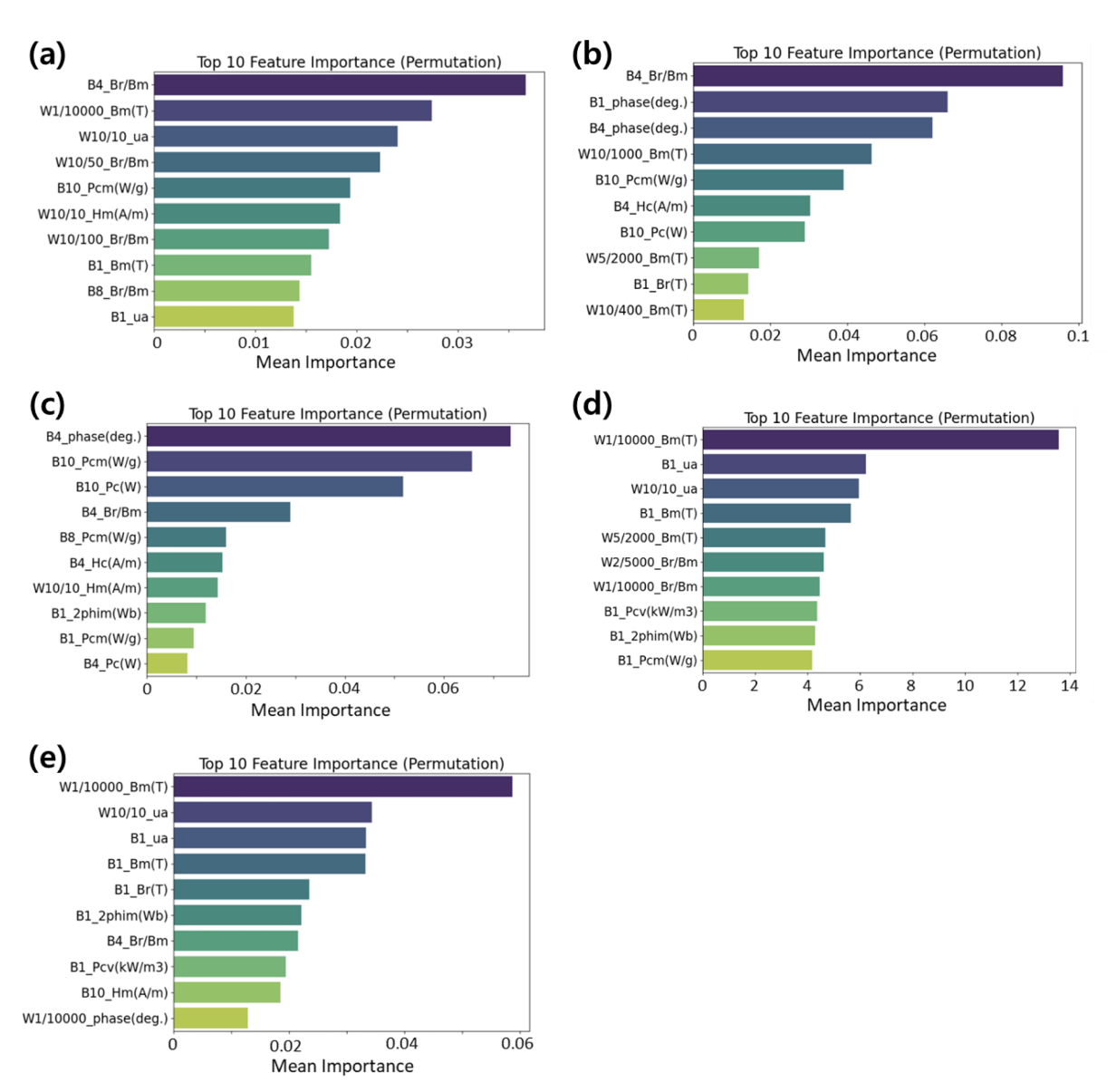


Fig. 7. (Color online) PFI bar plot of each model (a) TPOT, (b) XGBoost, (c) RFR, (d) GPR, (e) DNN.

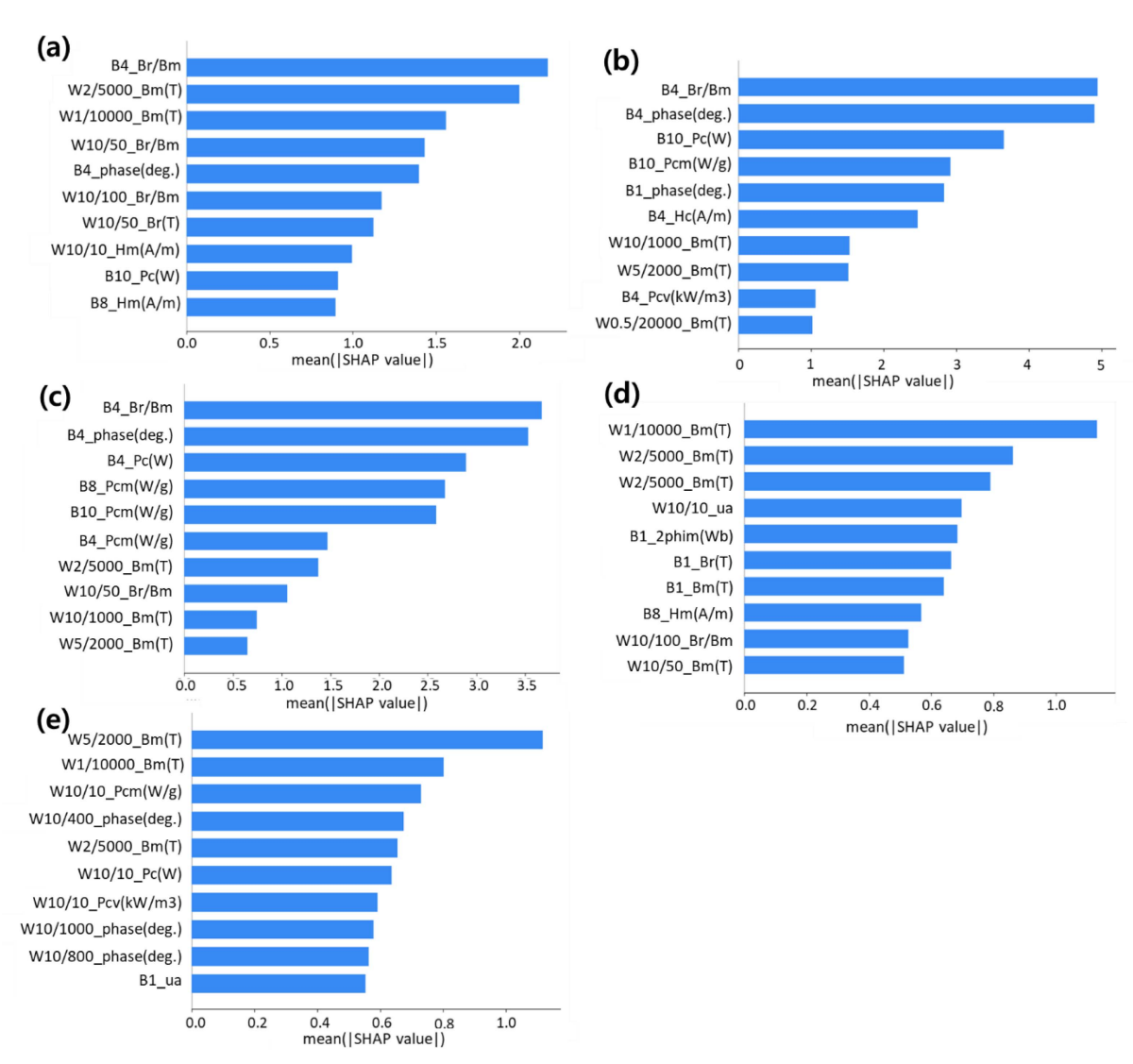


Fig. 8. (Color online) |SHAP| value bar plot of each model (a) TPOT, (b) XGBoost, (c) RFR, (d) GPR, (e) DNN.

and the relationship between each variable and grain size. The SHAP value of each variable indicates the importance of that variable to the model output. Fig. 7 shows the bar plot of the top 10 PFI values of each model, and Fig. 8 shows the input variables with the top 10 mean absolute SHAP values of each model.

Tables 6 and 7 present the results ranked after at least

10 iterations, summarizing the top five features in descending order of importance. In the tree-based model, the influence of magnetic property features measured at low frequency flux density such as B4_Br/Bm, B4_phase (deg.), B10_ $P_{cm}(W/g)$ is high. But, in the neural network-based models, features measured at specific core losses such as W1/10000_ $B_m(T)$, W10/10_ μ_a were more influential.

Table 6. Rank of PFI value.

TPOT	XGBoost	RFR	GPR	DNN
B4_Br/Bm	B4_Br/Bm	B4_phase(deg.)	W1/10000_Bm(T)	W1/10000_Bm(T)
W1/10000_Bm(T)	B1_phase(deg.)	B10_Pcm(W/g)	W10/10_ua	W10/10_ua
W10/10_ua	B4_phase(deg.)	B10_Pc(W)	B1_ua	B1_ua
W10/50_Br/Bm	W10/1000_Bm(T)	B4_Br/Bm	B1_Bm(T)	B1_Bm(T)
B10_Pcm(W/g)	B10_Pcm(W/g)	B8_Pcm(W/g)	B1_Br(T)	

Table 7. Rank of SHAP value.

TPOT	XGBoost	RFR	GPR	DNN
B4_Br/Bm	B4_Br/Bm	B10_Pcm(W/g)	W1/10000_Bm(T)	W5/2000_Bm(T)
W2/5000_Bm(T)	B4_phase(deg.)	B10_Pc(W)	W2/5000_Bm(T)	W2/5000_Bm(T)
W1/10000_Bm(T)	B10_Pc(W)	B4_phase(deg.)	B4_Br/Bm	W1/10000_Bm(T)
W10/50_Br/Bm	B10_Pcm(W/g)	B4_Br/Bm	W10/10_ua	W10/10_Pcm(W/g)
B4_phase(deg.)	B1_phase(deg.)	B8_Pcm(W/g)		W10/10_Pc(W)

According to the above paper [25], tree-based models learned structured data with higher performance than neural network-based models. Neural network-based models are not optimized for learning non-smooth patterns and are invariant to the rotation of each data feature. In contrast, tree-based models treat each feature separately, which is advantageous in low-information datasets and is considered appropriate for the dataset used in this paper. Thus, considering that the data used in this study involve a relatively small sample size and require the identification of nonlinear relationships, tree-based models were found to be more suitable. This is also

supported by their superior performance, as presented in Table 5. To summarize the results of the models, only three tree-based models: TPOT, XGBoost, and RFR were selected.

In the three tree-based models, the impact of each feature on grain size was visually represented through graphs using the dot plot, waterfall plot, force plot, and dependence plot provided by the SHAP library. These graphs highlight the factors that most significantly impact the model's predictive decisions and illustrate the relationships between each variable and the predicted values.

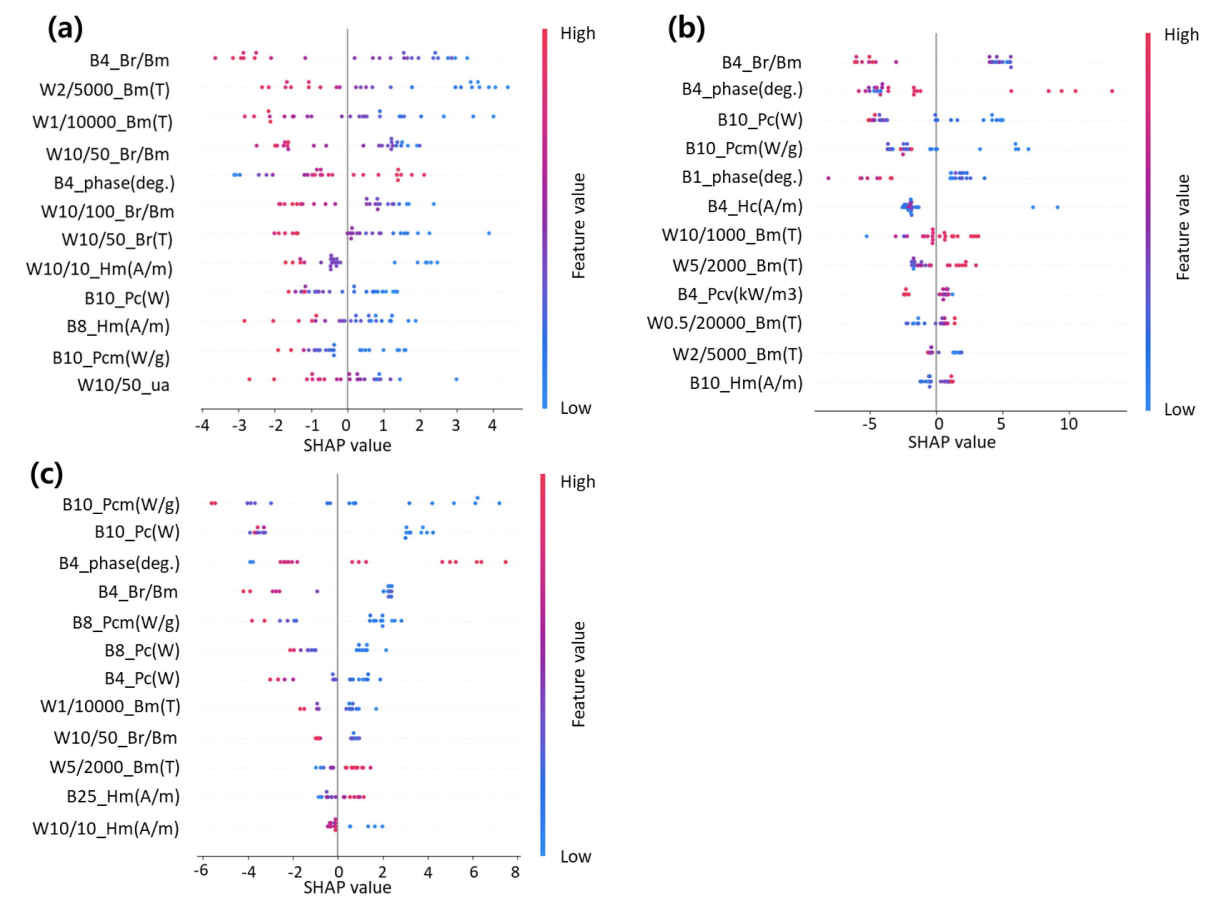


Fig. 9. (Color online) SHAP value dot plot (a) TPOT dot plot, (b) XGBoost dot plot, (c) RFR dot plot.

Fig. 9 is a dot plot visualization of SHAP values. Red dots indicate when the variable has a high value, and blue dots indicate when the variable has a low value. The horizontal position of a dot on the graph is the SHAP value of that data point, which shows the magnitude and direction of the variable's impact on the model's predictions. A point to the right (positive value) indicates that the variable has an effect that increases the model's predicted value, while a point to the left (negative value) indicates that the variable has an effect that decreases the predicted value. From the TPOT and XGBoost SHAP dot plots in Fig. 9(a) and Fig. 9(b), it is evident that B4_Br/

Bm is distributed with red dots at negative values, which means that high values of B4_Br/Bm are associated with negative SHAP values, while low values correspond to positive SHAP values. The positive SHAP value means that the low values of B4_Br/Bm contributed to the increase in model predicted value, and B4_Br/Bm is inversely related to grain size. According to previous studies [26, 27], having a large grain size facilitates the movement of the magnetic domain wall and the formation of multiple magnetic domains, which improves the soft magnetism characteristics of high permeability, low coercive force, and low remanent flux, and these changes

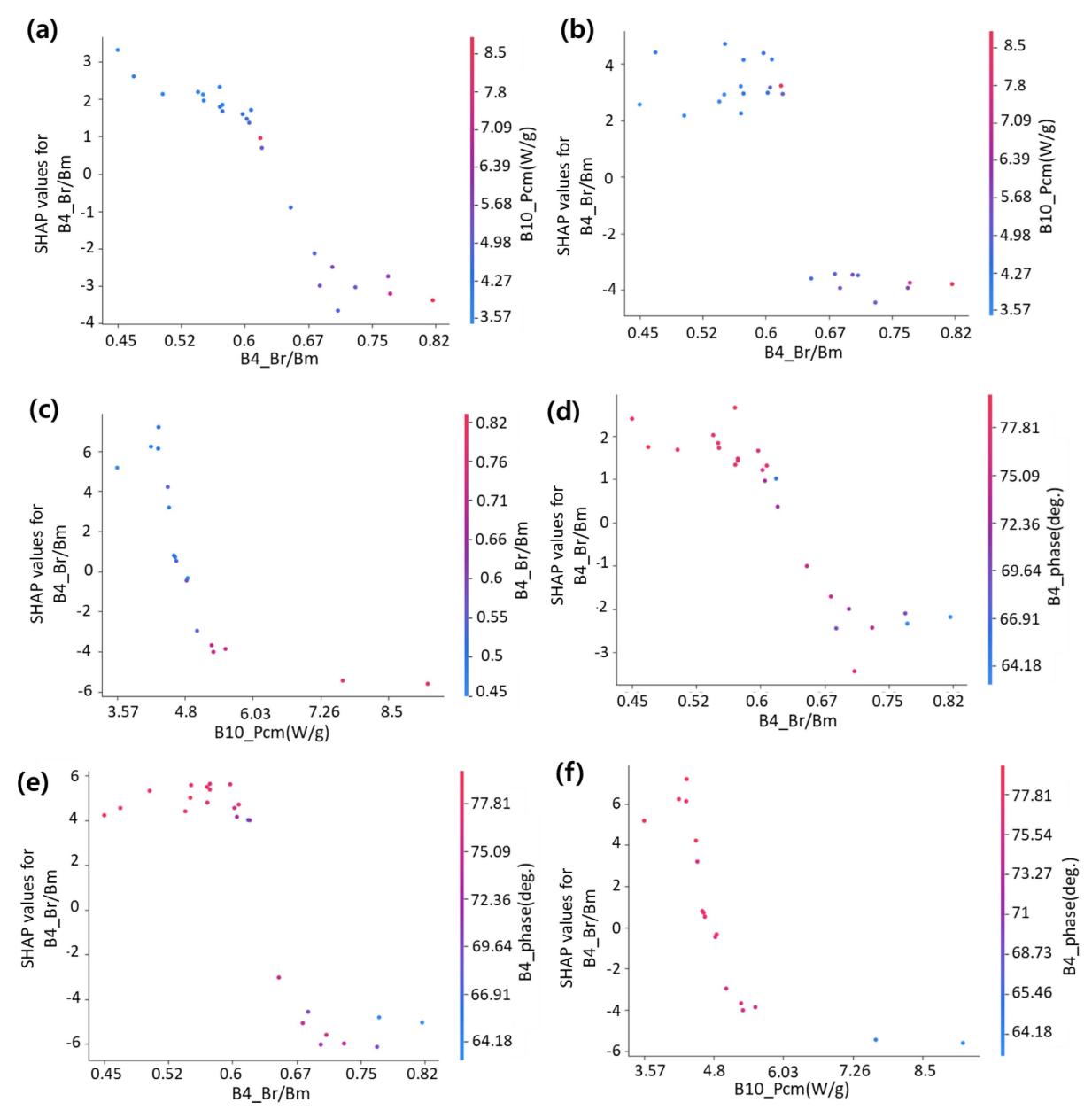


Fig. 10. (Color online) SHAP value dependence plot between B4_Br/Bm and B10_Pcm(W/g) (a) TPOT dot plot, (b) XGBoost dot plot, (c) RFR dot plot and B4_Br/Bm and B4_phase(deg.) (d) TPOT dot plot, (e) XGBoost dot plot, (f) RFR dot plot.

may slightly increase the maximum flux density (B_m) but not significantly [28], and significantly decrease the remanent flux density (B_r) and remanence ratio (Br/Bm)[26]. The RFR dot plot in Fig. 9(c) shows that the $B10_{P_{cm}}(W/g)$ input variable has the largest SHAP value, and the small values (blue dots) are distributed in the positive SHAP value, which is inversely related to the grain size. In addition, the relative difference in core loss decreases with increasing frequency. The decrease in core loss is 16-21% between 50 and 400 Hz and 4-8% for frequencies above 1000 Hz. This increases the explanatory ability of the model results by showing that the input variables at 50 Hz, the frequency of B4 and B10, have a stronger relationship with grain size, and that flux density has a stronger relationship with grain size than core loss, Remanence ratio (Br/Bm) and Core loss per mass $(P_{cm}(W/Bm))$ g)) have a stronger relationship with grain size, which is supported by previous studies.

By comparing the PFI and SHAP values of the three tree-based models in Tables 6 and 7, it was determined that the highly ranked and frequently occurring input variables contribute the most to grain size prediction, and these key variables are identified as B4_Br/Bm, B4_phase (deg.) and B10 $P_{cm}(W/g)$. The SHAP Dependence Plot shows the interaction of factors that affect prediction. It plots the actual value of a variable and its corresponding SHAP value on the x-axis and y-axis to show how the variable affects the final prediction result. The colored points compare the magnitude of the variable values and provide a visual analysis of the SHAP dependence of the important inputs in the model. Fig. 10 shows the interaction of the three variables which have the highest PFI and SHAP values in the three models. In Fig. 10(a), (b), the variable B4 Br/Bm, changes the sign of SHAP value based on the value of 0.63. The relationship with variable B10_ $P_{cm}(W/g)$ shows that B10_ $P_{cm}(W/g)$ is generally smaller (blue dots) when B4 Br/Bm < 0.75, indicating that the two variables exhibits a proportional relationship. In the RFR model in Fig. 10(c), the input variable with the highest SHAP value is B10 $P_{cm}(W/g)$ so the x-axis and dot plot variables are switched. When the value of B10_ $P_{cm}(W/g)$ is below 4.8, B4_Br/Bm also has the same tendency as Fig. 10(a) and (b) in that the value is small and most of the data is clustered. Br/Bm represents the ratio of the remaining magnetic flux when the external magnetic field is removed from the magnetized state. It indicates the vertical height ratio of the hysteresis loop, and a high Br/Bm means that even when the magnetic field H becomes zero, a significant amount of B remains. This implies a strong hysteresis effect and difficulty in demagnetization. In this case, P_{cm} refers to the total core loss, which includes hysteresis loss, eddy current loss, and anomalous loss. A larger B-H loop area means greater hysteresis loss, which makes it is theoretically reasonable that Br/Bm and P_{cm} are in a proportional relationship. In Fig. 10(d), (e), and (f), the change of SHAP value of B4_Br/Bm and B10_ P_{cm} , as well as their relationship with B4_phase(deg.). First, B4_Br/Bm, B4_phase and B10_ P_{cm} are observed to be inversely related. The phase difference is expressed as an angle and is calculated as follows:

Phase Difference(
$$\phi$$
) = $\phi_B - \phi_H$ (5)

The phase difference is in the range $0^{\circ} < \phi < 90^{\circ}$, where ϕ_B is the phase angle of the flux density B and ϕ_H is the phase angle of the magnetic field H. The presence of a phase angle means that the flux density does not respond immediately to changes in the magnetic field. The presence of a phase angle means that flux density does not respond instantaneously to changes in the magnetic field. This delay is due to microscopic magnetic interaction and energy loss mechanisms (hysteresis loss, eddy current loss) inside the magnetic material. Hysteresis loss is the energy loss caused by the rearrangement of the magnetic domain not keeping up with the changes in the magnetic field. Eddy current loss is the loss of energy due to the fact that the eddy current induced by the change in magnetic field generates an additional magnetic field, which acts in opposition to the original magnetic field. Both phenomena are related to the delay in flux density and magnetic field. B_r This directly leads to an increase in P_{cm} because the wider the loop, the greater the energy loss. Additionally, the relationship between the phase difference (ϕ) and the dissipated energy is observed [29].

$$w = \oint H dB \approx \frac{B_m H_m}{2} \sin \phi \tag{6}$$

Where B_m and H_m are the maximum values of each signal. The loss energy w is proportional to P_{cm} , so eventually, as ϕ increases, $\sin \phi$ increases, resulting in a larger loss energy and P_{cm} . Ideally, in the absence of loss, $\phi=0$ (B and H are in-phase), whereas in the presence of loss, H leads, B lags, and $\phi>0$. In general, in soft magnetism materials, the phase difference is small on the order of a few degrees (sec), but in high Si steel or nanocrystalline alloys, research is being done to minimize ϕ to a few or less by reducing losses [30]. Compared to Fig. 10(d), (e), and (f), the relationship between Br/Bm and phase(deg.) appears to be somewhat inconsistent with theoretical expectations. This suggests that further research is needed.

Fig. 11 shows which magnetic conditions contain the

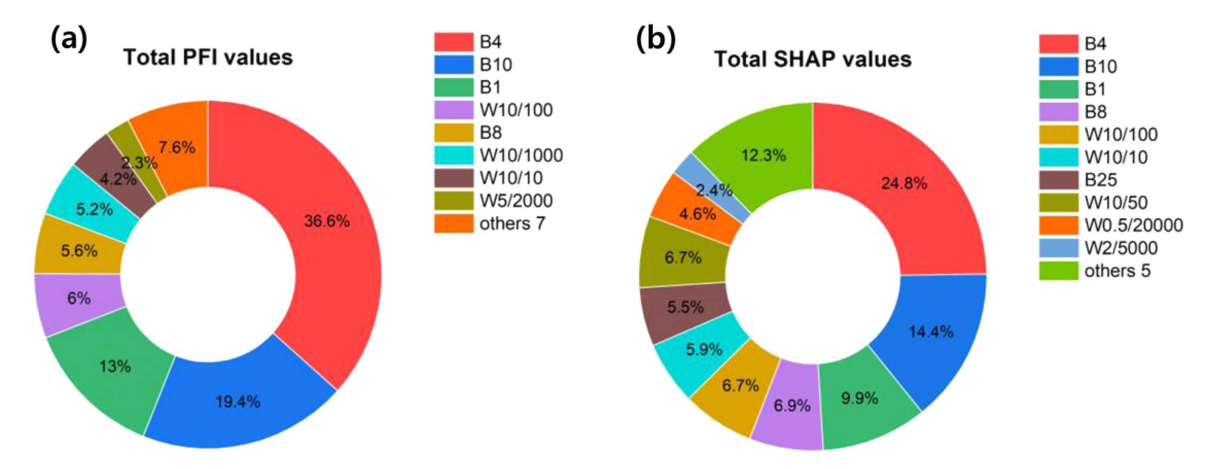


Fig. 11. (Color online) Pie chart of the sum of the three models (TPOT, XGBoost, RFR) of (a) PFI value (b) SHAP value.

highest and most explanatory variables by summing the PFI and SHAP values from three tree-based models based on magnetic criteria. In both Fig. 11(a) and (b), the plots indicate that the magnetic properties measured at B1, B4, and B10 show relatively high importance, accounting for approximately 70% and 50% of the explanatory capability, respectively. Furthermore, the consistently high importance of magnetic properties at flux densities of 100, 400, and 1000 A/m for B1, B4, and B10 provides insight into the effectiveness of measurements across a wide range of conditions, excluding high flux density regions. These findings suggest that grain size prediction may be efficiently supported by magnetic measurements at three flux density levels.

With the aim of improving the model's applicability, the relationship between the input variables in B1, B4, and B10 and grain size was organized into a linear expression. The regression coefficients were organized using the linear regression model ElasticNet.

$$D = 10.05x_{B1_Bm} + 7.11x_{B1_Br} - 3.13x_{B1_Hm} + \cdots - 9.23x_{B10_Br/Bm} - 7.5x_{B10_2phim}$$
 (7)

The following formula is a linear regression equation that predicts grain size using 11 magnetic properties measured at B1, B4, and B10, for a total of 33 variables. In the above equation, the input variables $B4_H_m(A/m)$, $B10_phase(deg.)$ have a regression coefficient of 0. This means that it has almost no significance, and it is also an input variable that does not exist in Tables 6 and 7. The R2 value of this linear model is 0.61, which is lower compared to the performance of the previously developed models. This indicates a limitation in predicting the complex behavior of grain size using a linear equation. As a result, using the same variables, three previously

Table 8. Final model performance comparison.

	TPOT	XGBoost	RFR
R2	0.66	0.65	0.74
RMSE	16.49	16.59	16.27

selected tree-based models were applied to consider nonlinear relationships through machine learning.

Table 8 compares the performance of the three models for predicting grain size using 11 magnetic properties measured in B1, B4, and B10, for a total of 33 variables. The hyperparameter optimization for new input variables is the same as the method used. The results show that the RFR model is the most effective in predicting grain size. Compared to Table 5, a decrease of approximately 0.09 and 0.14 in the R2 values of TPOT and XGBoost, respectively, was observed, along with an increase in RMSE of up to 3.95. In contrast, the performance of the RFR model was found to remain almost unchanged. Regression tree finds the best split based on MSE (or other impurity) at each node. Random forests, on the other hand, have the structural property that at each split during the learning process, they select the input variable with the largest impurity reduction from a randomly selected subset of features. Because of this property, even though feature importance is not explicitly evaluated during modeling, low-importance input variables are used relatively little or ignored in the model and, as a result, do not have a significant impact on model performance [19, 31]. In Table 6, which measures feature importance when modeling with 165 input variables, the magnetic properties of B4 and B10 are the highest, which explains why almost the same input variables were rated as highly important as the models created in Table 8, and the fact

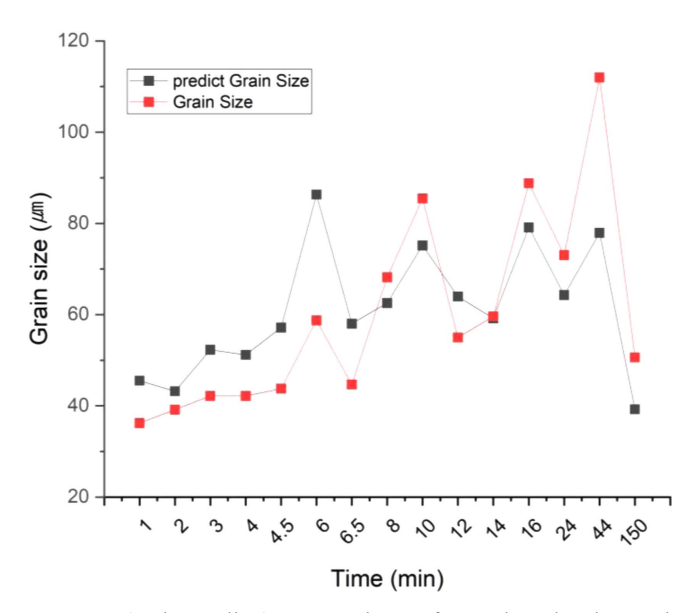


Fig. 12. (Color online) Comparison of actual grain size and predicted values by the RFR model at 1000 °C.

that these input variables were used as the split criterion explains why almost similar performance was obtained.

Using the RFR model, Fig. 12 presents a comparison between the actual grain size measured at 1000 °C and the grain size predicted by the model. The actual grain size exhibits a trend similar to the predicted values. The average residual between the actual and predicted values is 13.07 μ m. Notably, the grain size begins to increase after a heat treatment time of 44 minutes, indicating the occurrence of recrystallization and grain growth phenomena. At this condition, the RFR model showed its largest prediction error of 34.05 µm. This appears to be due to the limited amount of data available for grain sizes exhibiting such phenomena, resulting in lower predictive capability. Excluding the grain size error at 44 minutes, the average error for the remaining data is 10.8 μ m, suggesting that additional data collection in this range may improve model performance. In addition, the model was developed using magnetic data under three flux density conditions: 100, 400, and 1000 A/m. This suggests that measuring additional magnetic data between 100 and 1000 A/m such as data at 800 A/m, may lead to a model with improved predictive performance. Although creating a model to predict grain size using various magnetic properties data after measuring magnetic properties multiple times may have a higher prediction accuracy, in order to increase the utilization of the model and reduce the prediction cost, a model was created to predict grain size using magnetic properties data measured at B1, B4, and B10, the three most important magnetic measurement fix parameters selected in Fig. 11.

4. Conclusions

In this study aimed to non-destructively predict the grain size of non-oriented electrical steel by analyzing the complex relationships between various magnetic properties and grain size using machine learning. To address the black-box problem of the models, XAI techniques such as PFI and SHAP were applied. Among the five models (TPOT, XGBoost, RFR, DNN, and GPR), the XGBoost model showed the highest performance with an R2 of 0.79 and RMSE of 12.64. Overall, the tree-based models (TPOT, XGBoost, RFR) outperformed the neural networkbased models (DNN, GPR) in terms of both R2 and RMSE. Based on the characteristics of the data, which required learning non-smooth patterns, the three treebased models were selected for PFI and SHAP analysis. In all three models, the most influential input variables were magnetic properties measured at low-frequency flux densities, such as B4 Br/Bm, B4 phase(deg.) and B10 $P_{cm}(W/g)$. Through SHAP dot plots and dependence plots, the influence of these variables, their relationship with grain size, and their interactions were analyzed, and the results coincide with magnetic theories. By summing the PFI and SHAP values of the three models, it was confirmed that the variables under the magnetic conditions B1, B4, and B10 accounted for about 70% of the model explanation ratio. Using 33 magnetic properties measured under these three conditions, the RFR model achieved a performance of R2 = 0.74 and RMSE = 16.27. When comparing the predicted grain size with experimental values under the 1000 °C heat treatment condition, an average error of 13.07 μ m was observed. Through this study, it was demonstrated that grain size could be effectively predicted with only three magnetic measurements, improving practical applicability. This suggests that grain size is measurable and controllable in real time during continuous electrical steel production.

Acknowledgment

This research are results of a study on the "Busan Regional Innovation System & Education (RISE)" Project, supported by the Ministry of Education and Busan Metropolitan City.

This work was also supported the Pukyong National University Industry-university Cooperation Foundation's 2024 (202315460001).

Statements and Declarations

The authors report there are no competing interests to declare.

References

- [1] L.-Z. An, Y.-P. Wang, G.-D. Wang, and H.-T. Liu, J. Magn. Magn. Mater. **567**, 170358 (2023).
- [2] Z.-H. Li, S.-K. Xie, G.-D. Wang, and H.-T. Liu, Mater. Charact. 183, 111593 (2022).
- [3] E. J. Gutiérrez-Castañeda, and A. Salinas-Rodríguez, J. Magn. Magn. Mater. **323**, 2524 (2011).
- [4] M. Shiozaki and Y. Kurosaki, Journal of Materials Engineering 11, 37 (1989).
- [5] M. F. de Campos, T. Yonamine, M. Fukuhara, F. J. G. Landgraf, C. A. Achete, and F. P. Missell, IEEE Trans. Magn. 42, 2812 (2006).
- [6] H. Pan, Z. Zhang, and J. Xie, J. Magn. Magn. Mater. 401, 625 (2016).
- [7] N. Leuning, S. Steentjes, and K. Hameyer, J. Magn. Magn. Mater. 469, 373 (2019).
- [8] N. S. Reddy, A. K. Prasada Rao, M. Chakraborty, and B. S. Murty, Materials Science and Engineering: A 391, 131 (2005).
- [9] J. He, C. Gao, X. Wang, J. Yang, Q. Tian, and X. Guan, Ultrasonics **141**, 107334 (2024).
- [10] R. Xue, X. Wang, Q. Yang, D. Xu, Y. Sun, J. Zhang, and S. Krishnaswamy, Applied Acoustics 180, 108125 (2021).
- [11] S. M. Lundberg, S.-I. Lee, Proceedings of the 31st International Conference on Neural Information Processing Systems, Long Beach, USA (2017), pp. 4766-4777.
- [12] R. Alizadehsani, S. S. Oyelere, S. Hussain, S. K. Jagatheesaperumal, R. R. Calixto, M. Rahouti, M. Roshanzamir, and V. H. C. De Albuquerque, IEEE Access 12, 35796 (2024).
- [13] K. K. Kırboğa, S. Abbasi, and E. U. Küçüksille, Chem. Biol. Drug Des. 102, 217 (2023).
- [14] M. Botlani-Esfahani and M. R. Toroghinejad, J. Serb.

- Chem. Soc. 77, 669 (2012).
- [15] J. Jeon, N. Seo, J. G. Jung, H. S. Kim, S. B. Son, and S. J. Lee, Journal of Materials Research and Technology 21, 1408 (2022).
- [16] T. Chen and T. He, xgboost: eXtreme Gradient Boosting (2024). https://cran.r-project.org/web/packages/xgboost/vignettes/xgboost.pdf
- [17] J. Schmidhuber, Neural Networks **61**, 85 (2015).
- [18] R. S. Olson, N. Bartley, R. J. Urbanowicz, and J. H. Moore, GECCO 2016 - Proceedings of the 2016 Genetic and Evolutionary Computation Conference, 485 (2016).
- [19] L. Breiman, Mach. Learn. 45, 5(2001).
- [20] C. E. Rasmussen, Lecture Notes in Computer Science (Including Subseries Lecture Notes in Artificial Intelligence and Lecture Notes in Bioinformatics) 3176, 63 (2004).
- [21] H. Kaneko, Analytical Science Advances 3, 278 (2022).
- [22] F. Pedregosa, G. Varoquaux, A. Gramfort, V. Michel, B. Thirion, O. Grisel, M. Blondel, P. Prettenhofer, R. Weiss, V. Dubourg, J. Vanderplas, A. Passos, D. Cournapeau, M. Brucher, M. Perrot, and E. Duchesnay, Journal of Machine Learning Research 12, 2825 (2011).
- [23] J. E. Guyer, D. Wheeler, and J. A. Warren, Comput. Sci. Eng. 11, 6 (2009).
- [24] S. M. Allen and J. W. Cahn, Acta Metallurgica **20**, 423 (1972).
- [25] L. Grinsztajn, E. Oyallon, and G. Varoquaux, Advances in Neural Information Processing Systems **35**, 507 (2022).
- [26] J. T. Park and J. A. Szpunar, J. Magn. Magn. Mater. 321, 1928 (2009).
- [27] Y. Du, R. O'Malley, and M. F. Buchely, Applied Sciences **13**, 6097 (2023).
- [28] K. M. Lee, S. Y. Park, M. Y. Huh, J. S. Kim, and O. Engler, J. Magn. Magn. Mater. **354**, 324 (2014).
- [29] G. Mörée and M. Leijon, J. Magn. Magn. Mater. 609, 172163 (2024).
- [30] X. Cui, J. Zhou, J. Pang, K. Qiu, X. Li, J. You, D. Yang, and J. Bu, J. Appl. Phys. 136, 135103 (2024).
- [31] G. Louppe, arXiv:1407.7502v3 (2014).